Biosensors and Bioelectronics xxx (xxxx) xxx

Contents lists available at ScienceDirect

Biosensors and Bioelectronics

journal homepage: http://www.elsevier.com/locate/bios

# Highly sensitive detection of hydrazine by a disposable, Poly(Tannic Acid)-Coated carbon electrode

Al-Monsur Jiaul Haque [a,1,2], Sumit Kumar [b,2], Jonathan Sabaté del Río [b,2], Yoon-Kyoung Cho [a,b,*]

[a] Department of Biomedical Engineering, School of Life Sciences, Ulsan National Institute of Science and Technology (UNIST), Ulsan, 44919, Republic of Korea
[b] Center for Soft and Living Matter, Institute for Basic Science (IBS), Ulsan, 44919, Republic of Korea

ARTICLE INFO

*Keywords:*
Electrode modification
Bioconjugation
Tannic acid
Enzymatic polymerization
Hydrazine

ABSTRACT

We propose an electrochemical sensor based on the enhanced electrocatalytic oxidation exhibited on a functionalized poly(tannic acid) coating to detect hydrazine. Tannic acid, a naturally abundant and low-cost polyphenol, was enzymatically polymerized with horseradish peroxidase and subsequently adsorbed on a disposable screen-printed carbon electrode with a short incubation time (30 min). The fabrication method proved to be reproducible (4.2 % relative standard deviation), with the sensors displaying high sensitivity ($7 \times 10^{-3}$ μA $mm^{-2}$ $\mu M^{-1}$) and selectivity even in the presence of various common interfering agents. The low detection limit (100 nM) and robustness of the sensor demonstrated its suitability for environmental applications. It can be used to quantify hydrazine in tap and river water samples.

## 1. Introduction

Hydrazine (HZ), an important biochemical reagent and a strong reducing agent, is widely used in numerous industrial applications, including pesticides, pharmaceuticals, fuel cells, foaming agents, emulsifiers, blowing agents, textile dyes, corrosion inhibitors, and as propellant fuel for spacecraft. However, HZ is very toxic, colorless, flammable, easily water-soluble, and can cause severe injuries to lungs, liver, kidneys, brain, and spinal cord in humans (Channon et al., 2015; Gu and Camden, 2015; Krittayavathananon et al., 2014; Umar et al., 2013; Zhang et al., 2015). In addition, HZ has been classified as a probable human carcinogen in group B2 by the United States Environmental Protection Agency, which has set its threshold limit value as low as 10 ppb (312 nM) (Gu and Camden, 2015). Therefore, the detection and monitoring of trace amounts of HZ discharged in the environment is very important for environmental and biological analysis.

To date, numerous methods have been reported on the sensitive and selective trace-level detection of HZ, including spectrophotometric, titrimetric, electrophoretic, chromatographic, potentiometric, amperometric, flow injection analysis with chemiluminescence, surface-enhanced Raman spectroscopy (SERS), and fluorescence-based techniques (Bharath et al., 2016; Channon et al., 2015; Gao et al., 2017; Gu and Camden, 2015; Jena and Raj, 2007; Krittayavathananon et al., 2014; Lee et al., 2016; Li and Lin, 2007; Li et al., 2011; Peng and Liang, 2017; Roy et al., 2017; Shang et al., 2012; Sharel et al., 2016; Tang et al., 2012; Umar et al., 2013; Zhang et al., 2015; Zhao et al., 2016). Among these methods, electrochemical techniques are superior in terms of simplicity, sensitivity, speed, low cost, and being compatible with miniaturized portable devices for on-site analysis. However, direct electrochemical oxidation of HZ on bare conventional electrode surfaces leads to sluggish kinetics and high over-potentials. Hence, modification of the electrode surfaces with any catalytic material is essential for the sensitive detection of HZ and low over-potential. To this end, various inorganic and organic materials, including metal nanoparticles (Bharath et al., 2016)(Krittayavathananon et al., 2014)(Zhao et al., 2016), semiconductor nanoparticles (Umar et al., 2013), hexacyanoferrate salts, metal phthalocyanine and porphyrin complexes (Gu et al., 2016), carbon nanotubes (Gu et al., 2016; Zhao et al., 2016), and graphene-oxides-based nanocomposites (Gao et al., 2017; Sakthinathan et al., 2017; Zhang et al., 2017)(Gu et al., 2016; Krittayavathananon

* Corresponding author. Department of Biomedical Engineering, School of Life Sciences, Ulsan National Institute of Science and Technology (UNIST), Ulsan, 44919, Republic of Korea.
*E-mail address:* ykcho@unist.ac.kr (Y.-K. Cho).
[1] Current address: Department of Chemistry, Pusan National University, Busan 46241, Republic of Korea.
[2] The authors are equally contributed.

https://doi.org/10.1016/j.bios.2019.111927
Received 7 September 2019; Received in revised form 17 November 2019; Accepted 25 November 2019
Available online 26 November 2019

et al., 2014; Peng and Liang, 2017; Zhang et al., 2009) have been used due to their good electrocatalytic properties. However, the use of these materials has drawbacks such as complex synthesis, the use of organic solvents, complex preparation steps, high-cost, and low reproducibility. Recently, the mussel-inspired surface modification by self-polymerization of dopamine in alkaline pH was used to transform a relatively low electrocatalytic indium tin oxide electrode into a suitable catalytic HZ detection platform (Lee et al., 2016). However, the use of poly(dopamine) as a coating material has limitations such as high-cost, slow-rate of the self-polymerization, strong coloration, and interference of its abundant amine groups for quantifying or characterizing immobilized molecules (Abouelmagd et al., 2016). Plant polyphenols, tannic acid (TA) in particular, are naturally abundant, cheap materials that share some properties with dopamine due to their large number of hydroxyl groups and multiple aromatic rings that bind strongly to surfaces of different materials through covalent bonds and non-covalent interactions (Sileika et al., 2013). This property has been used to generate electrode coatings on a number of different electrode materials for direct bioconjugation of antibodies, cells or DNA capture probes, and detection of electroactive small molecules (Kumar et al., 2019).

Here we present a simple, rapid, and cheap electrode functionalization method for HZ detection based on an enhanced electrocatalytic oxidation of HZ on poly(tannic acid)-functionalized electrodes. The poly (tannic acid) was prepared by a rapid (30 min) enzymatic polymerization with horseradish peroxidase (HRP) and drop-casted on a disposable screen-printed carbon electrode (SPCE) with a short incubation period (30 min) (Fig. 1). The sensor showed good reproducibility with robust performance even in complex matrices such as tap water or river water, displaying high sensitivity and selectivity with a low detection limit (100 nM).

## 2. Experimental section

### 2.1. Materials, chemicals and electrochemical setup

Tannic acid, peroxidase from horseradish (HRP), hydrogen peroxide ($H_2O_2$), and hydrazine solution (35 wt % in $H_2O$) were purchased from Sigma-Aldrich. Tris-HCl (1.5 M, pH 8.8) was purchased from Biosesang Inc. River water sample was collected from the Taehwa River near UNIST in Ulsan, Korea. Unless otherwise stated, all reagent-grade chemicals were used as received, and ultrapure deionized water (18.2 MΩ cm) was used to prepare all buffer and aqueous solutions. Screen-printed carbon electrode chips containing four working electrodes (geometric area = 6.835 $mm^2$), a common counter electrode, and a common silver paste pseudo-reference electrode were purchased from Korea Total Printing Technology (KTP Tech) and DropSens. All electrochemical measurements were carried out in a three-electrode configuration using a potentiostat/galvanostat (VSP, BioLogic Science Instrument).

### 2.2. Preparation of poly(tannic acid) (p(TA)) solution

We carried out the enzymatic polymerization of TA following an optimized protocol. A 1 mL p(TA) solution was freshly prepared by mixing a 970 μL of 2 mg $mL^{-1}$ TA and a Tris-HCl buffer (10 mM pH 8.5) in a 10 μL of an HRP solution (100 μM). The reaction started after adding 20 μL of 1 M $H_2O_2$ followed by a short vortexing. The reaction products were characterized by UV–visible spectroscopy. The absorbance at 430 nm was followed to optimize the incubation time.

### 2.3. Preparation of p(TA)-coated electrode surfaces

Screen-printed carbon electrodes were electrochemically cleaned by cyclic voltammetry, scanning from 0 to 1.3 V in 0.5 M sulfuric acid 50 times at 0.5 V $s^{-1}$. 100 μL of p(TA) solution was drop-casted on the electrode surfaces and incubated for 30 min in a water-saturated atmosphere, followed by washing with a Tris-HCl buffer, water, and drying under a stream of $N_2$ gas. The p(TA)-coated SPCE was electrochemically oxidized by cyclic voltammetry in the Tris-HCl buffer (10 mM pH 8.5) at 50 mV $s^{-1}$.

### 2.4. Surface characterizations

The electrochemical oxidation of SPCE/p(TA) was also carried out by square wave voltammetry to obtain a well-resolved peak voltammogram of the p(TA) (pulse height = 30 mV, pulse width = 100 ms, step height = 4 mV, scan rate = 20 mV $s^{-1}$). The electrochemical active area of the coating, optimal p(TA) incubation time, electron transfer kinetics, and charge transfer resistance ($R_{CT}$) of each step were carried out in 2.5 mM $[K_4Fe(CN)_6]/[K_3Fe(CN)_6]$ solution with 1 M KCl as the supporting electrolyte by cyclic voltammetry and electrochemical impedance spectroscopy (0.1 MHz–0.1 Hz, 5-mV amplitude *vs.* open circuit potential, 50 logarithmically spaced measurements). Chemical composition was characterized by X-ray photoelectron spectroscopy (XPS) after each modification step. For the topographic characterization of the coating, p (TA) was prepared on a gold thin-film evaporated on glass and allowed to adsorb for 30 min. The topography of the coating was analyzed by atomic force microscopy (AFM) (Veeco Dimension 3100, Veeco, South Korea) in a non-contact tapping mode using <10-nm radius tips (Product #TAP300AL-G-10, NanoAndMore, USA) to determine the morphology and roughness of the coating. The thickness of the p(TA) coating was measured by an AFM tip-scratch test on the p(TA)-coated surface.

### 2.5. Electrochemical measurements

Electrochemical measurements of hydrazine were carried out in the Tris-HCl buffer (pH 8.5) by cyclic voltammetry (scan rate 50 mV $s^{-1}$ from 0 to 0.3 V *vs.* reference potential) and the reaction kinetics was evaluated by cyclic voltammetry at different scan rates.

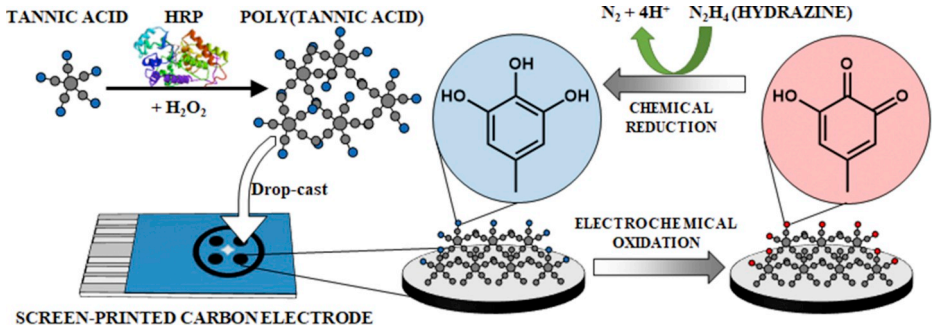


**Fig. 1.** Schematic representation of the electrocatalytic detection of hydrazine on poly(tannic acid)-coated, screen-printed carbon electrode surface.

## 3. Results and discussion

### 3.1. Choice of materials

To overcome the limitations associated with the high overpotential required for the electrochemical oxidation of HZ on bare electrode surfaces, many studies have proposed the modification of electrode surfaces with various materials like organic polymers, carbon nanomaterials, metal nanoparticles, metal oxides, and metal sulfides (*e.g.* PPy, PANI, rGO, AuNPs, PdNPs, AgNPs, ZnO, $SnO_2$, $Mn_2O_3$, $MoS_2$, and $NiCo_2S_4$). Although the good catalytic activities of these materials allow highly sensitive detection of HZ, synthesizing or preparing these materials usually requires several synthesis and electrode preparation steps, and the use of organic solvents with expensive chemicals. This increases the overall fabrication time and cost, whereas the added complexity is detrimental for the reproducibility. Herein we studied the electrocatalytic properties of p(TA) because it can be easily and quickly prepared using a naturally abundant and cheap material under mild reaction conditions.

### 3.2. Polymerization of TA

After the addition of hydrogen peroxide, HRP catalyzes the oxidative peroxidation of TA molecules, which in turn, react with other TA molecules and start the polymerization. The UV–Visible peaks corresponding to TA shifted to lower wavelengths due to the formation of quinone groups during the oxidative polymerization of the phenolic compounds (Fig. 2a) (Kawakita et al., 2009). Even though the solution turned dark brown within a few seconds (Fig. 2a), when we measured the absorbance at 430 nm, we observed that a plateau was reached after 30 min (Fig. S1). However, the negative control without HRP stayed colorless and yielded a minor increase in absorbance due to self-polymerization of TA.

### 3.3. Characterization of the p(TA)-coated SPCE

The chemical composition of the bare SPCE, SPCE/p(TA), SPCE/p$(TA)_{ox}$ and SPCE/p$(TA)_{red}$ were characterized by high-resolution XPS. The C1s spectra were analyzed and deconvoluted to fit Gaussian peak shapes after a Shirley baseline correction (Fig. 2b–c, Fig. S2). Five components could be identified corresponding to carbon atoms: C═C at ~284.2 eV, C–C at 284.9 eV, hydroxyl/epoxy/ether group C–O at ~285.8 eV, carbonyl carbon C═O at 287 eV, and carboxylate carbon O═C–O at ~288.7 eV. The binding energies were higher on the SPCE/p(TA)ox (Fig. 2c) than the SPCE/p(TA)red (Fig. 2b), corresponding to the conversion of hydroxyl groups (C–O/OH) from gallic acid residues to quinone groups (C═O). This shift was reversible by reducing with hydrazine or electrochemically oxidizing the electrodes (Fig. S2).

The topographic characterization of the p(TA)-coated SPCE (SPCE/p(TA)) revealed a grainy surface with a root mean square of the roughness (Sq) of 6.9 nm, with the grain sizes in the range 80–120 nm, corresponding to the presence of the HRP enzymes trapped on and within the p(TA) coating during the polymerization. The thickness of the p(TA) films characterized by a scratching test with the AFM tip was ~50 nm (Fig. 2d).

The electrode kinetics were evaluated by cyclic voltammetry at different scan rates in the presence of a diffusible redox pair $[K_4Fe(CN)_6]/[K_3Fe(CN)_6]$. Although the oxidation-reduction peak-to-peak distance increased slightly with increasing scan rate (Fig. 2e), the current was proportional to the square root of the scan rate, as expected for a diffusion-controlled process, and linear between 10 and 200 mV $s^{-1}$ (Fig. 2f). Interestingly, the peak-to-peak distance of the SPCE/p(TA) was similar to the SPCE, with the current peak observed on the coated electrodes being only 4.6–12 % smaller than the bare SPCE. Considering the thickness of the p(TA) coating (~50 nm), this suggests that the ferro/ferricyanide redox couple was reacting with the surface of the p(TA) layer, not with the underlying carbon electrode. Otherwise, we would

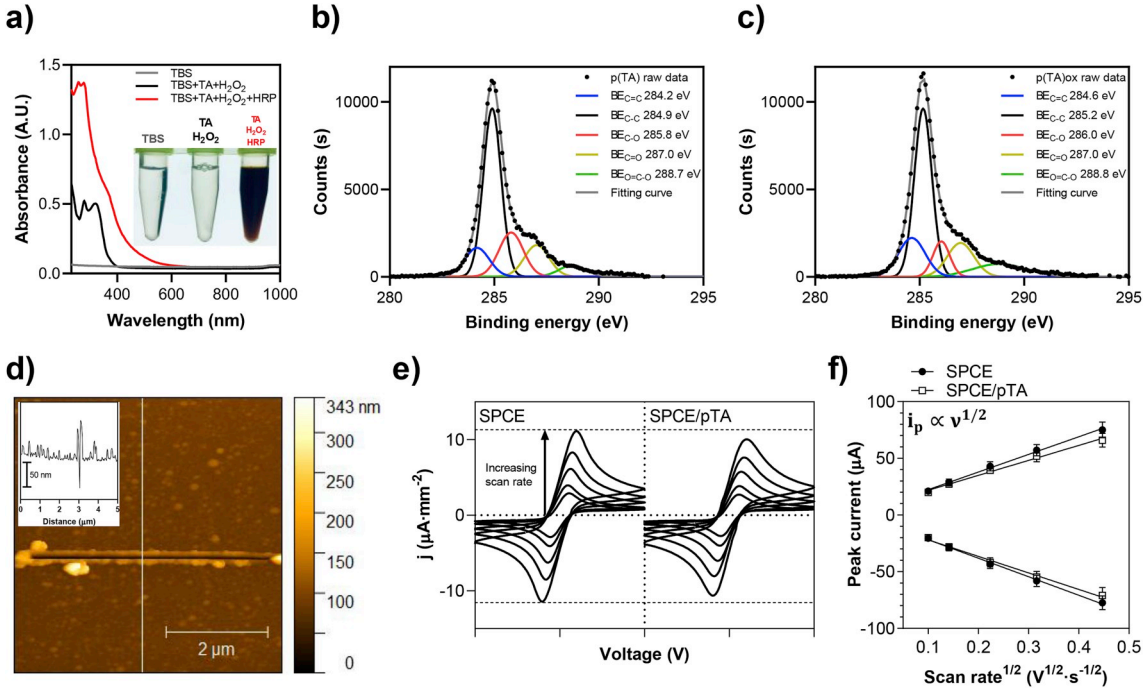


**Fig. 2.** (a) UV–Visible spectra of TBS, TA, and p(TA), and a picture of the solutions. (b) XPS spectra of C1s from SPCE/p(TA) and (c) SPCE/p$(TA)_{ox}$. (d) AFM topography and tip-scratch test of an evaporated gold surface covered with p(TA) solution. The inset shows the extracted profile corresponding to the white line in the topography (~50 nm thick coating). (e) Voltammograms of SPCE (left) and SPCE/p(TA) (right) of an equimolar solution of 2.5 mM ferri/ferrocyanide at different scan rates (10–200 mV $s^{-1}$). (f) Extracted oxidation/reduction peak currents from the voltammograms shown in (e) plotted versus the square root of the scan rate (n = 4). The error bars represent the standard deviation of the mean. (For interpretation of the references to color in this figure legend, the reader is referred to the Web version of this article.)

expect a sluggish reaction with broader peak-to-peaks and smaller current peaks due to the limited diffusion of the species towards the electrode surface. The electroactive area of the electrodes was estimated before and after the p(TA) coating by evaluating the peak current of the voltammograms at different scan rates using the Randles-Sevçik equation (Elgrishi et al., 2018):

$$i_p = 0.446nFAC^0 \cdot \left(\frac{nF\nu D_0}{RT}\right)^{\frac{1}{2}} \quad (1)$$

where n is the number of electrons transferred in the redox event (n = 1), A ($cm^2$) is the electrode geometric surface area, $D_0$ ($cm^2\ s^{-1}$) is the diffusion coefficient of the analyte ($D = 7.6 \times 10^{-6}$ cm $s^{-1}$), and $C_0$ (mol $cm^{-3}$) is the bulk concentration of the analyte ($C_0 = 2.5 \times 10^{-6}$ mol $cm^{-3}$). The area of the SPCE was estimated to be 8.38 $mm^2$, corresponding to a roughness factor (Rf) of 1.22, whereas the area of the SPCE/p(TA) was 7.12 $mm^2$ (Rf = 1.04).

Charge transfer resistance ($R_{CT}$) was estimated after each electrode modification step by fitting the impedance spectra from the Nyquist plots (Fig. 3a) to a Randles equivalent circuit (Fig. 3b). The $R_S$ models the resistance of the solution, the constant phase element (CPE) (non-ideal capacitance) models the double layer capacitance and the $R_{CT}$ (in parallel), and the Warburg element ($Z_W$) models the diffusion of electroactive species in a solution. The SPCE showed an initial increased $R_{CT}$ after being coated with p(TA) (Fig. 3c). This value gradually decreased with the incubation time of p(TA) on the SPCE, reaching a local minimum after 30 min (Fig. 3c). Typically, for an insulating coating, we would expect an increase of $R_{CT}$ over time as more material is deposited on the surface until a plateau is reached or the electrode becomes passivated. In this case, we have a coating with a delocalized π electron system which grants enhanced electron-transfer properties (Akkaya et al., 2018; Çakıroğlu and Özacar, 2017). Therefore, the optimum p(TA) incubation time is a compromise between the enhanced electron transfer kinetics from the material deposited and the passivation due to the thickness.

### 3.4. Electrochemical oxidation of SPCE/p(TA) to SPCE/p(TA)$_{ox}$

The first anodic square wave voltammograms of p(TA)-coated SPCE surfaces in the Tris-HCl buffer (10 mM pH 8.5) show two oxidation peaks at 0.16 and 0.47 V (Fig. 3e) that can be attributed to the oxidation of hydroxyl groups from the catechol and gallic acid residues of p(TA) to their corresponding quinone form p(TA)$_{ox}$ (Fig. 3f) (Chikere et al., 2019). No reduction peak was observed, even at scan rates of 5 V $s^{-1}$, and no further oxidation was observed in subsequent scans, indicating that the oxidation of p(TA) is electrochemically irreversible as previously observed by other groups (Maerten et al., 2017; Wan et al., 2007). After the electrochemical oxidation of p(TA) on the SPCE, a significant irreversible drop is observed in the $R_{CT}$ (Fig. 3d), suggesting that the process is followed by an internal cross-link from nearby TA molecules. Only residues on the surface of the coating are exempt from this process and can be reverse oxidized or reduced, therefore participating in later electrocatalytic processes. Furthermore, the $R_{CT}$ drop after the electrochemical oxidation of p(TA) is expected due to the formation of quinone groups and cross-linking of internal TA groups, yielding to a larger delocalized π electron system (Akkaya et al., 2018; Çakıroğlu and Özacar, 2017).

### 3.5. The electrocatalytic reaction of SPCE/p(TA)$_{ox}$ with hydrazine

The cyclic voltammograms obtained at bare (Fig. 4a) SPCE in a Tris-HCl buffer in the absence of HZ or the presence of 100 μM HZ only show a small capacitive current without any oxidation peak due to the slow electron transfer kinetics and high over-potential required for the electrochemical oxidation of HZ on a bare electrode surface. In the presence of hydrazine, the electrochemically oxidized and coated electrode SPCE/p(TA)$_{ox}$, undergoes a chemical reduction to regenerate the quinone groups into hydroxyl groups SPCE/p(TA)$_{red}$. Therefore, the electrode can be oxidized again by cyclic voltammetry. This is a reversible process, and the charge transfer resistance increases after the hydrazine reduction, and decreases after the electrochemical oxidation

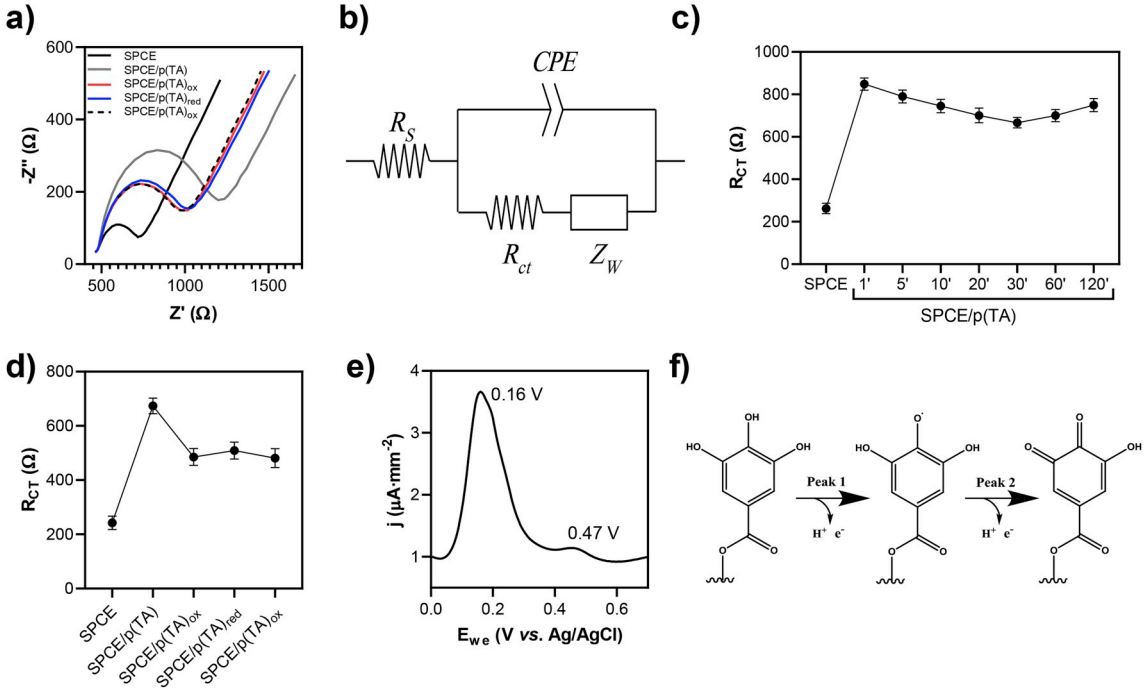


**Fig. 3.** (a) Nyquist plot of the electrochemical impedance spectra recorded after different electrode modifications. (b) Randles equivalent circuit used to estimate the charge transfer resistance from the impedance spectra. (c) Charge transfer resistance of the bare SPCE and the SPCE/p(TA) at different incubation times (Nyquist plots not shown). (d) Charge transfer resistance estimated from the Nyquist plots in "(a)" for different electrode modifications. (e) Square wave voltammetry of SPCE/p(TA) in Tris-HCl buffer showing the two oxidation peaks corresponding to (f) the conversion of hydroxyl groups from the gallic acid residues in TA to quinone forms.

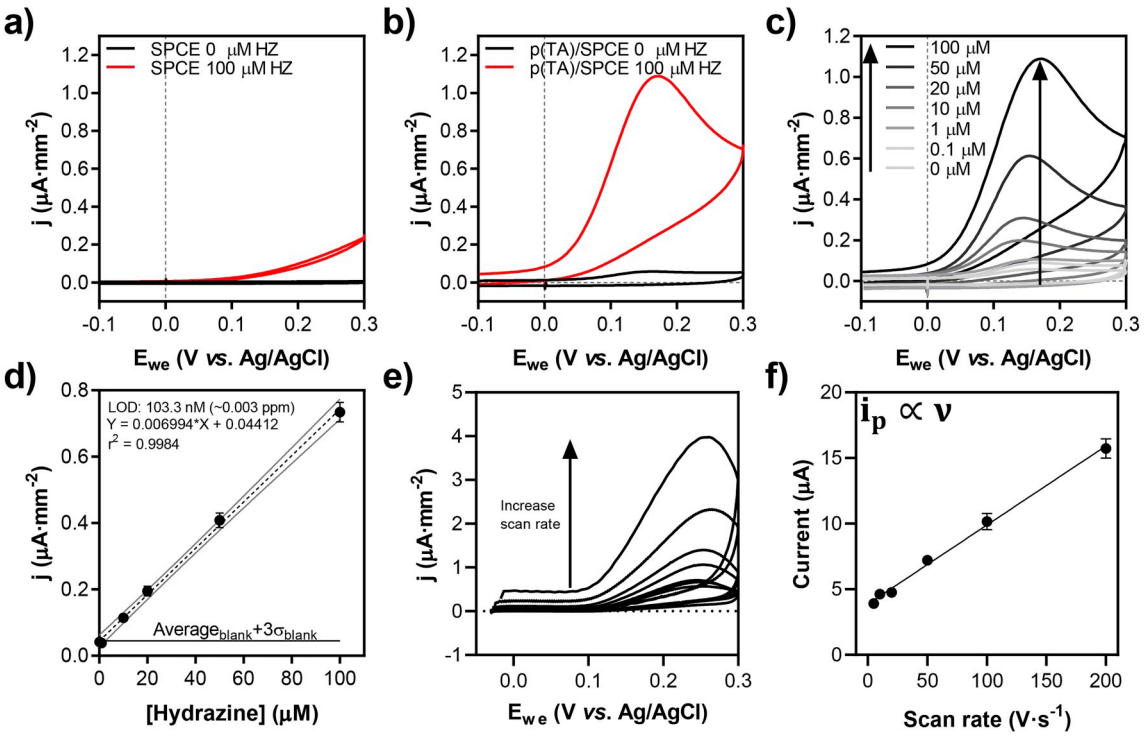


**Fig. 4.** (a) Cyclic voltammograms at bare and (b) p(TA)-modified SPCE surfaces in 10 mM Tris-buffer (pH 8.5) without (black lines) and with 100 μM Hydrazine (red lines). (c) Cyclic voltammograms at p(TA)-modified SPCE in a 10 mM Tris-buffer (pH 8.5) containing a range of different concentrations from 0 to 100 μM of hydrazine. (d) Calibration plot of HZ. The dots represent the average values of three independent measurements using three different electrodes. The error bars indicate a standard deviation from the average values. (e) Cyclic voltammograms at SPCE/p(TA)ox in a 100 μM hydrazine at different scan rates (10–200 mV $s^{-1}$) and (f) Extracted oxidation peak currents versus the scan rate. The dots represent the average values of four independent measurements using four different electrodes. The error bars indicate a standard deviation from the average values. (For interpretation of the references to color in this figure legend, the reader is referred to the Web version of this article.)

(Fig. 3d).

When poising the SPCE/$p(TA)_{ox}$ electrode at 0.3 V in the presence of HZ, a constant current is produced by the redox cycling reaction between HZ and the p(TA) surface; first, $p(TA)_{red}$ is electrochemically oxidized to $p(TA)_{ox}$, which is chemically reduced back to $p(TA)_{red}$ by HZ, and the process is repeated cyclically (Fig. 1).

### 3.6. Quantitative analysis, reproducibility, and selectivity of the sensor

The performance of the sensor was assessed by measuring the oxidation peak current at different concentrations of HZ (Fig. 4c). The oxidation peak current increased linearly with an increase in HZ concentration from 0.1 to 100 μM (Fig. 4d). The system showed good linearity with a sensitivity of $7{\cdot}10^{-3}$ μA $mm^{-2}$ $μM^{-1}$, a limit of detection of 100 nM (~0.003 ppm) and a limit of quantification of 6.9 μM (~0.22

**Table 1**
Comparison of detection performances of some different electrode materials used for the electrochemical detection of hydrazine.

| Electrode materials | Sensitivity (μA $cm^{-2}$ $μM^{-1}$) | Detection limit (μM) | Linear range (μM) | Reference |
|---|---|---|---|---|
| rGO/PdNPs | - | 0.007 | 0.04–200 | Krittayavathananon et al. (2014) |
| Au/CdS | 89 | 0.061 | 0.1–1.0 | Umar et al. (2013) |
| GCE/SWCNHs/AuNPs | - | 1.1 | - | Zhao et al. (2016) |
| Hap/AuNPs | 0.5 | 0.017 | 0.5–1429 | Bharath et al. (2016) |
| PDA-rGO | 0.158 | 0.01 | 0.03–100 | Peng and Liang (2017) |
| GCE/PPy/AuNPs | 0.126 | 0.2 | - | Li and Lin (2007) |
| HAP-rGO | 4.21 | 0.4 | - | Gao et al. (2017) |
| $Au/Ni_3$ | 0.136 | 0.07 | 0.2–50 | Gu et al. (2016) |
| CNF-GCE/PdNPs | 0.0086 | 2.9 | 10–4000 | Zhang et al. (2009) |
| rGO/PdNPs-β-CD | 0.95 | 0.028 | 0.05–1600 | Sakthinathan et al. (2017) |
| ITO/AuNPs@NC-ZnO | - | 0.004 | 0.05–10 | Zhang et al. (2017) |
| CMG/AuNC | 0.0377 | 0.5 | 6–30 | Daemi et al. (2017) |
| GCE/$NiCo_2S_4$ | 179.1 | 0.6 | 1.7–7800 | Duan et al. (2019) |
| GCE/CB-DHP/Au–Pd | 0.0824 | 0.23 | 2.5–88 | Deroco et al. (2018) |
| GCE/OMC/AgNPs | - | 0.027 | 0.08–33.8 | Rofouei et al. (2018) |
| SPCE/p(TA) | 0.7 | 0.1 | 0.1–100 | This work |

PdNP: palladium nanoparticles, rGO: reduced graphene oxide, CdS: Cadmium selenide, Au: gold, AuNP: gold nanoparticles, SWCNHs: single-wall carbon nanohorns, GCE: glassy carbon electrode, HAp: hydroxyapatite, PPy: polypyridine, HAP: hydroxyapatite, $Ni_3$: trinuclear Ni(II) complex, CNF: carbon nanofiber, β-CD: beta-cyclodextrin, NC: N-doped carbon, ZnO: zinc oxide, ITO: indium tin oxide, AuNC:gold nanocage, CMG: chemically modified graphene, $NiCo_2S_4$: Nickel cobalt sulfide, Au–Pd/CB: carbon black supported Au–Pd core–shell structured nanoparticles, DHP: dihexadecylphosphate, AgNPs: silver nanoparticles, OMC: ordered mesoporous carbon.

ppm) estimated from the mean of the blank plus, three or ten times the standard deviation of the blank, respectively. This detection limit is well below the threshold values set by different organizations such as the United States Environmental Protection Agency and Occupational Safety and Health Administration. The catalytic oxidation of 100 μM of HZ on SPCE/p(TA)ox electrodes was characterized by cyclic voltammetry at different scan rates to determine the nature of the redox process (Fig. 4e), finding that the process is kinetically controlled as the oxidation peak current is linear to the scan rate (Fig. 4f). Therefore, the oxidation of hydrazine is not limited by the diffusion of the species towards the electrode, but clearly defined as a surface process on the SPCE/p(TA)ox.

The analytical performance of the sensor is comparable in terms of the limit of detection and sensitivity to many other reported electrochemical HZ sensors (Table 1). Additionally, the sensor fabrication method is much simpler with the naturally abundant and inexpensive tannic acid. The excellent performance of the sensor could be attributed to: 1) The rich active sites (-OH) of p(TA) which allow strong adsorption and contact of HZ on the electrode/electrolyte interface. 2) The high amplification of the signal current by the redox cycling reaction between p(TA)ox and HZ. The reproducibility of the sensor was evaluated by measuring the current response towards the detection of HZ with three different sensing surfaces under the same conditions, showing a reproducibility of 4.2 % of the relative standard deviation (RSD).

The selectivity of the sensor was assessed by detecting HZ in the presence of some commonly coexisting interfering agents such as $Na^+$, $K^+$, $Mg^{2+}$, $Ca^{2+}$, $Zn^{2+}$, $Cl^-$, $SO_4^{2-}$, $CO_3^{2-}$, $NO_2^-$, $NO_3^-$, and $PO_4^{2-}$, and organic compounds such as glucose, sucrose, and urea. As shown in Fig. 5a, the voltammetric peak current responses to the interfering agents were negligible, and the response to the HZ in the presence of the interfering agents at concentrations >200 higher than hydrazine was similar to the response obtained without any interfering agent. Fig. 5b shows the chronoamperometric response of the p(TA)-functionalized SPCE after adding HZ and other interfering agents to a continuously stirred Tris-HCl buffer. After successive additions of HZ, a significant increase in current response was observed, whereas the addition of interfering agents such as KCl, $KNO_3$, $KH_2PO_4$, $NH_4Cl$, $NaNO_2$, $Na_2CO_3$, $MgSO_4$, $FeCl_3$, glucose, sucrose, and urea yielded no considerable variation in the catalytic current, showing an excellent selective catalytic oxidation towards HZ. A small drop in current was observed after the addition of $ZnCl_2$, indicating that $Zn^{2+}$ was reduced by hydrazine, as the standard reduction potential of Zn is −0.7618 V and the reaction is thermodynamically favorable. Therefore, this reaction may have reduced the concentration of hydrazine and the signal observed. More importantly, the catalytic current increases again when HZ was further added into the solution containing all the potential interfering agents, thus confirming that our sensor has good selectivity towards HZ detection.

### 3.7. Study of matrix effect in tap and river water

The robustness and suitability of our sensors for environmental analysis were tested with the analysis of water samples, including tap and river water (collected from Taehwa River in Ulsan, Korea) (Fig. 5c and d). Different concentration of HZ was spiked on the samples for analysis using the standard addition method, finding 0.6 and 1.2 μM of hydrazine in the samples of tap water and the river water, respectively. As shown in Table 2, the recovery values for river and tap water are in the acceptable analytical range 95–120 %. Furthermore, with RSD being in the range 1–9 %, indicates the p(TA)-functionalized sensors' potential application in the analysis of HZ in tap and river samples. However, both samples exhibited a recovery rate higher than 120 % at 100 μM of

**Table 2**
Detection of hydrazine added and found in tap and river samples (n = 4).

| Samples | Added (μM) | Found (μM) | Recovery (%) | RSD (%) (n = 4) |
|---|---|---|---|---|
| Tap water | 10 | 9.27 | 95 | 10 |
| | 20 | 21 | 104 | 2 |
| | 50 | 58.28 | 115 | 5 |
| | 100 | 125.65 | 125 | 1 |
| River water | 10 | 9.8 | 98 | 9 |
| | 20 | 22.1 | 109 | 5 |
| | 50 | 60.3 | 120 | 4 |
| | 100 | 127.7 | 127 | 2 |

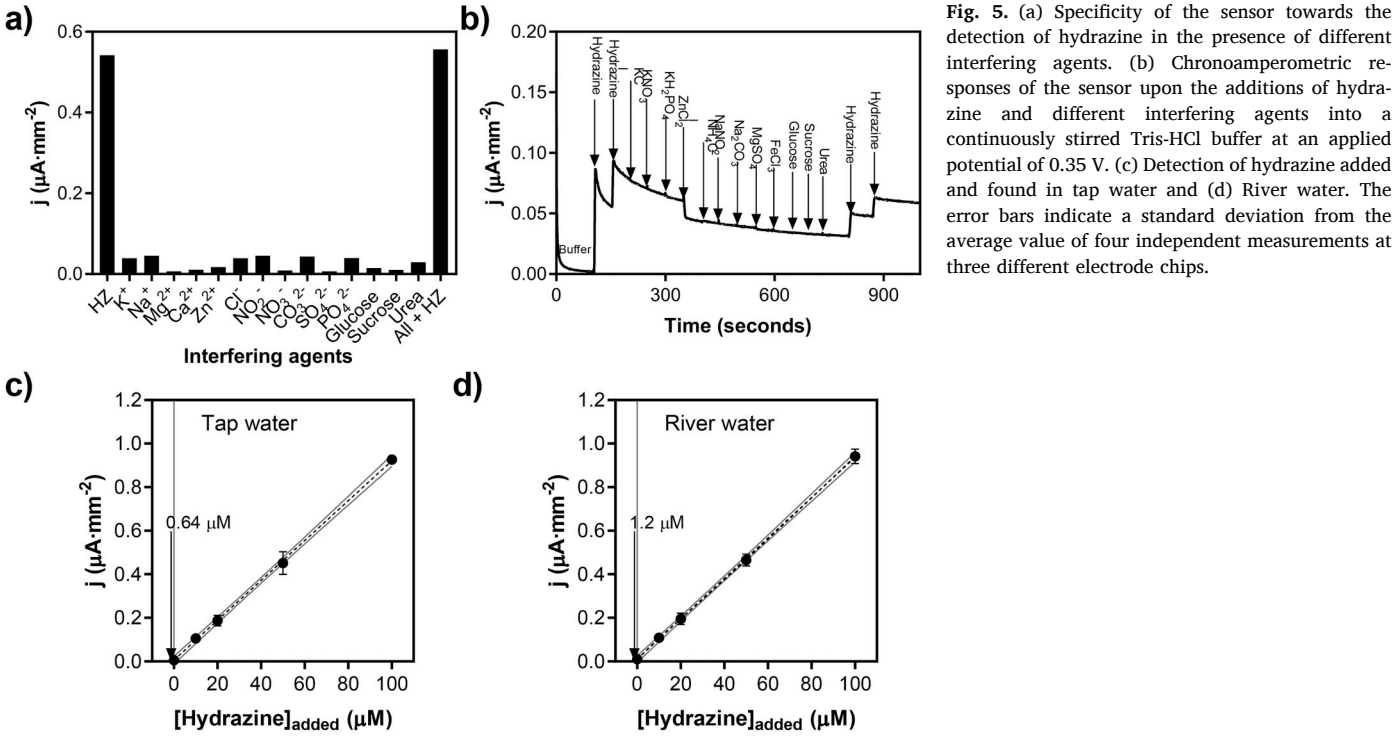


**Fig. 5.** (a) Specificity of the sensor towards the detection of hydrazine in the presence of different interfering agents. (b) Chronoamperometric responses of the sensor upon the additions of hydrazine and different interfering agents into a continuously stirred Tris-HCl buffer at an applied potential of 0.35 V. (c) Detection of hydrazine added and found in tap water and (d) River water. The error bars indicate a standard deviation from the average value of four independent measurements at three different electrode chips.

hydrazine, which might indicate a matrix effect at higher ranges.

## 4. Conclusions

We have developed a simple and rapid electrode functionalization method for HZ detection based on the enhanced electrocatalytic oxidation exhibited on poly(tannic acid)-coated screen-printed carbon electrodes. The electrodes were functionalized by drop-casting an enzymatically polymerized, cheap, and naturally abundant polyphenol, tannic acid, for a short period of time (30 min). The electrodes achieved a robust, sensitive, and selective hydrazine quantification with a detection limit of 100 nM (~0.003 ppm), which is well below the threshold limit value set by the US EPA (10 ppb), and comparable to the ones from other (nanomaterial-based) reported methods. The good recoveries of hydrazine in real water samples with low standard deviations in an acceptable analytical range show the practical application of our sensors.

## Declaration of competing interest

The authors declare that they have no known competing financial interests or personal relationships that could have appeared to influence the work reported in this paper.

## CRediT authorship contribution statement

**Al-Monsur Jiaul Haque:** Conceptualization, Methodology, Validation, Investigation, Writing - original draft. **Sumit Kumar:** Conceptualization, Methodology, Validation, Investigation, Writing - review & editing. **Jonathan Sabaté del Río:** Conceptualization, Methodology, Validation, Investigation, Writing - original draft. **Yoon-Kyoung Cho:** Investigation, Supervision, Writing - review & editing, Project administration, Funding acquisition.

## Acknowledgments

This work was supported by the taxpayers of South Korea through the Institute for Basic Science (project code IBS-R020-D1), Republic of Korea.

## Appendix A. Supplementary data

Supplementary data to this article can be found online at https://doi.org/10.1016/j.bios.2019.111927.

## References

Abouelmagd, S.A., Meng, F., Kim, B.-K., Hyun, H., Yeo, Y., 2016. ACS Biomater. Sci. Eng. 2 (12), 2294–2303.
Akkaya, B., Çakiroğlu, B., Özacar, M., 2018. ACS Sustain. Chem. Eng. 6 (3), 3805–3814.
Bharath, G., Naldoni, A., Ramsait, K.H., Abdel-Wahab, A., Madhu, R., Alsharaeh, E., Ponpandian, N., 2016. J. Mater. Chem. 4 (17), 6385–6394.
Çakıroğlu, B., Özacar, M., 2017. Electroanalysis 29 (12), 2719–2726.
Channon, R.B., Joseph, M.B., Bitziou, E., Bristow, A.W., Ray, A.D., Macpherson, J.V., 2015. Anal. Chem. 87 (19), 10064–10071.
Chikere, C.O., Faisal, N.H., Kong Thoo Lin, P., Fernandez, C., 2019. J. Solid State Electrochem. 23 (6), 1795–1809.
Daemi, S., Ashkarran, A.A., Bahari, A., Ghasemi, S., 2017. Sens. Actuators, B 245, 55–65.
Deroco, P.B., Melo, I.G., Silva, L.S., Eguiluz, K.I., Salazar-Banda, G.R., Fatibello-Filho, O., 2018. Sens. Actuators, B 256, 535–542.
Duan, C., Dong, Y., Sheng, Q., Zheng, J., 2019. Talanta 198, 23–29.
Elgrishi, N., Rountree, K.J., McCarthy, B.D., Rountree, E.S., Eisenhart, T.T., Dempsey, J. L., 2018. J. Chem. Educ. 95 (2), 197–206.
Gao, F., Wang, Q., Gao, N., Yang, Y., Cai, F., Yamane, M., Gao, F., Tanaka, H., 2017. Biosens. Bioelectron. 97, 238–245.
Gu, X., Camden, J.P., 2015. Anal. Chem. 87 (13), 6460–6464.
Gu, X., Li, X., Wu, S., Shi, J., Jiang, G., Jiang, G., Tian, S., 2016. RSC Adv. 6 (10), 8070–8078.
Jena, B.K., Raj, C.R., 2007. J. Phys. Chem. C 111 (17), 6228–6232.
Kawakita, H., Hamamoto, K., Ohto, K., Inoue, K., 2009. Ind. Eng. Chem. Res. 48 (9), 4440–4444.
Krittayavathananon, A., Srimuk, P., Luanwuthi, S., Sawangphruk, M., 2014. Anal. Chem. 86 (24), 12272–12278.
Kumar, S., Haque, A.-M.J., Sabaté del Río, J., Gautam, S., Cho, Y.-K., 2019. Biosens. Bioelectron. 127, 50–56.
Lee, J.Y., Nguyen, T.L., Park, J.H., Kim, B.-K., 2016. Sensors 16 (5), 647.
Li, J., Lin, X., 2007. Sens. Actuators, B 126 (2), 527–535.
Li, J., Xie, H., Chen, L., 2011. Sens. Actuators, B 153 (1), 239–245.
Maerten, C., Lopez, L., Lupattelli, P., Rydzek, G., Pronkin, S., Schaaf, P., Jierry, L., Boulmedais, F., 2017. Chem. Mater. 29 (22), 9668–9679.
Peng, H., Liang, C., 2017. Fullerenes, Nanotub. Carbon Nanostruct. 25 (1), 29–33.
Rofouei, M.K., Khoshsafar, H., Bagheri, H., Kalbasi, R.J., 2018. Int. J. Environ. Anal. Chem. 98 (2), 156–170.
Roy, B., Halder, S., Guha, A., Bandyopadhyay, S., 2017. Anal. Chem. 89 (19), 10625–10636.
Sakthinathan, S., Kubendhiran, S., Chen, S.-M., Sireesha, P., Karuppiah, C., Su, C., 2017. Electroanalysis 29 (2), 587–594.
Shang, L., Zhao, F., Zeng, B., 2012. Electroanalysis 24 (12), 2380–2386.
Sharel, E., Kim, Y.-R., Perry, D., Bentley, C.L., Unwin, P.R., 2016. ACS Appl. Mater. Interfaces 8, 30458–30466.
Sileika, T.S., Barrett, D.G., Zhang, R., Lau, K.H.A., Messersmith, P.B., 2013. 52(41), 10766-10770.
Tang, Y.-Y., Kao, C.-L., Chen, P.-Y., 2012. Anal. Chim. Acta 711, 32–39.
Umar, A., Kansal, S.K., Mehta, S.K., 2013. Sens. Actuators, B 188, 372–377.
Wan, H., Zou, Q., Yan, R., Zhao, F., Zeng, B., 2007. Microchim. Acta 159 (1), 109–115.
Zhang, H., Huang, J., Hou, H., You, T., 2009. Electroanalysis 21 (16), 1869–1874.
Zhang, J., Ning, L., Liu, J., Wang, J., Yu, B., Liu, X., Yao, X., Zhang, Z., Zhang, H., 2015. Anal. Chem. 87 (17), 9101–9107.
Zhang, Y., Han, T., Wang, Z., Zhao, C., Li, J., Fei, T., Liu, S., Lu, G., Zhang, T., 2017. Sens. Actuators, B 243, 1231–1239.
Zhao, S., Wang, L., Wang, T., Han, Q., Xu, S., 2016. Appl. Surf. Sci. 369, 36–42.